T2R2 東京科学大学 リサーチリポジトリ
Science Tokyo Research Repository

論文 / 著書情報
Article / Book Information

Title	Design of Checkerboard-Distortion-Free Multidimensional Multirate Filters
Authors	Tomohiro TAMURA, Masaki KATO, Toshiyuki YOSHIDA, AKINORI NISHIHARA
Citation	IEICE Transactions on Fundamentals of Electronics, Communications and Computer Sciences, Vol. E81-A, No. 8, pp. 1598-1606
Pub. date	1998, 8
URL	http://search.ieice.org/
Copyright	(c) 1998 Institute of Electronics, Information and Communication Engineers

Powered by T2R2 (Science Tokyo Research Repository)

IEICE TRANS. FUNDAMENTALS, VOL. E81–A, NO. 8 AUGUST 1998

PAPER Special Section on Digital Signal Processing

Design of Checkerboard-Distortion-Free Multidimensional Multirate Filters

Tomohiro TAMURA†, Masaki KATO††, *Nonmembers*, Toshiyuki YOSHIDA†††, *and* Akinori NISHIHARA††††, *Members*

SUMMARY This paper discusses a design technique for multidimensional (M-D) multirate filters which cause no checkerboard distortion. In the first part of this paper, a necessary and sufficient condition for M-D multirate filters to be checkerboard-distortion-free is derived in the frequency domain. Then, in the second part, this result is applied to a scanning line conversion system for television signals. To confirm the effectiveness of the derived condition, band-limiting filters with and without considering the condition are designed, and the results by these filters are compared. A reducibility of the number of delay elements in such a system is also considered to derive efficient implementation.

key words: *multidimensional filters, multirate filters, checkerboard distortion, Scanning line conversion*

1. Introduction

Multirate signal processing techniques have been applied to many areas such as filter banks, multiplexed signal transmission, adaptive signal processing, and spectral estimation, and so on [1]–[4].

Upsamplers and downsamplers, which are basic building blocks in multirate signal processing, are periodically time-variant systems, and thus have characteristics quite different from those of time-invariant systems. For example, in a stable linear time-invariant filter, the output for a step input converges to a certain value determined from its DC gain. A multirate filter having upsamplers, however, often causes a periodic distortion for a step input, known as *checkerboard distortion*.

A necessary and sufficient condition for avoiding such kind of distortion has been derived in the temporal or spatial domain, which is a relation between DC gain of each polyphase component [5]–[8]. In one-dimensional (1-D) multirate systems, Harada et al. [8] and the authors [6] have shown that this condition is equivalent to a suitable placement of zeros in the frequency domain.

Manuscript received December 10, 1997.
Manuscript revised March 2, 1998.

†The author is with Monitor Products Dept., Display Systems Div., B & P Co., Sony Corporation, Osaki West Technology Center, Tokyo, 141–0032 Japan.
††The author is with DVD Products Division, Texas Instruments Japan Ltd., Tokyo, 108–0023 Japan.
†††The author is with the Faculty of Eng., Tokyo Institute of Technology, Tokyo, 152–8552 Japan.
††††The author is with Center for Research and Development of Educational Technology, Tokyo Institute of Technology, Tokyo, 152–8552 Japan.

On the other hand, in multidimensional (M-D) systems, Harada et al. have shown a sufficient condition for an M-D filter to be checkerboard-distortion-free, and proposed a checkerboard-distortion-free filter structure [9]. Although this structure has an advantage that it is structurally insensitive to coefficient quantization, their condition is not a necessary and sufficient condition.

The purpose of this paper is to derive a condition for an M-D multirate filter to be checkerboard-distortion-free and to obtain its efficient hardware implementation. We first show that, for M-D filters, the checkerboard-distortion-free condition in the spatial domain can be also converted into the zero placement problem in the frequency domain [7]. As a practical application of this condition, a scanning line conversion system for television (TV) signals is considered. In such a system, a reduction of the number of delay elements for one direction is quite important from the viewpoint of hardware implementation. A condition for such reducibility is then investigated, from which an efficient implementation can be obtained.

In what follows, Sect. 2 briefly overviews M-D multirate systems. In Sect. 3, checkerboard distortion is investigated both in the spatial and frequency domains, and necessary and sufficient conditions for avoiding checkerboard distortion are derived. In Sect. 4, this condition is applied to a scanning line converter for TV signals, and its efficient implementation is considered. Finally, Sect. 5 concludes this paper.

2. Multidimensional Multirate System

2.1 Preparations

The following notations are utilized in this paper;

$\boldsymbol{n} = [n_1, \cdots, n_D]^T$	: D-dimensional (D-D) integer vector
$\boldsymbol{\omega} = [\omega_1, \cdots, \omega_D]^T$	: D-D angular frequency vector
$\boldsymbol{z} = [z_1, \cdots, z_D]^T$	: D-D z variable vector
$\mathcal{N}$	: set of all the D-D integer vectors
$\boldsymbol{V}, \boldsymbol{M}, \boldsymbol{L}$	: Nonsingular $D \times D$ integer matrix (Sampling matrix)

In addition to these, let $\boldsymbol{z}^{\boldsymbol{n}}$ denote $z_1^{n_1} z_2^{n_2} \cdots z_D^{n_D}$. By using this notation, D-D z transformation is written as

$$X(\boldsymbol{z}) = \sum_{\boldsymbol{n} \in \mathcal{N}} x(\boldsymbol{n}) \boldsymbol{z}^{-\boldsymbol{n}}, \tag{1}$$

where $x(\boldsymbol{n})$ is the D-D discrete signal obtained by sampling a continuous signal x_a with a sampling matrix $\boldsymbol{V}$; $x(\boldsymbol{n}) = x_a(\boldsymbol{V}\boldsymbol{n})$. By substituting $z_i = e^{j\omega_i}$ in Eq. (1), the frequency response $X(\boldsymbol{\omega})$ can be calculated.

Let $LAT(\boldsymbol{V})$ be the sampling lattice generated by the sampling matrix $\boldsymbol{V}$. Furthermore,

$$FPD(\boldsymbol{V}) = \boldsymbol{V}\boldsymbol{x} \quad (\boldsymbol{x} \in [0,1)^D)$$
$$SPD(\boldsymbol{V}) = \boldsymbol{V}\boldsymbol{x} \quad (\boldsymbol{x} \in [-1,1)^D)$$

are used to represent the fundamental region of the D-D lattice [2]. Since $FPD(\boldsymbol{V})$ includes $V = |\det \boldsymbol{V}|$ sampling points, let $\mathcal{N}(\boldsymbol{V})$ denote the set of these sampling points in $FPD(\boldsymbol{V})$. For $\boldsymbol{k}_i \in \mathcal{N}(\boldsymbol{V})$ $(i = 1, \cdots V)$, assume throughout in this paper that the first element $\boldsymbol{k}_1$ corresponds to $[0, \cdots, 0]^T$.

2.2 Multidimensional Sampling Rate Conversion

Figure 1 shows a general structure for multidimensional sampling rate converters. Except for a trivial case, we can assume $LAT(\boldsymbol{L}) \neq LAT(\boldsymbol{M})$. Let $v(\boldsymbol{n})$ be the upsampled version of the original input signal $x(\boldsymbol{n})$ with the upsampling matrix $\boldsymbol{L}$, which can be written as

$$v(\boldsymbol{n}) = \begin{cases} x(\boldsymbol{L}^{-1}\boldsymbol{n}) & (\boldsymbol{n} \in LAT(\boldsymbol{L})) \\ 0 & (\text{Otherwise}) \end{cases}. \tag{2}$$

Equation (2) is equivalent to

$$V(\boldsymbol{\omega}) = X(\boldsymbol{L}^T \boldsymbol{\omega}) \tag{3}$$

in the frequency domain, where $X(\boldsymbol{\omega})$ and $V(\boldsymbol{\omega})$ are the frequency response of $x(\boldsymbol{n})$ and $v(\boldsymbol{n})$, respectively. It should be pointed out that such an upsampling produces replica of the original spectra $X(\boldsymbol{\omega})$ on the lattice points $LAT(2\pi \boldsymbol{L}^{-T})$ in the frequency domain.

In the case of the downsampling with the downsampling matrix $\boldsymbol{M}$, the downsampled version of $w(\boldsymbol{n})$ is obtained as

$$y(\boldsymbol{n}) = w(\boldsymbol{M}\boldsymbol{n}), \tag{4}$$

which is rewritten in the frequency domain as

$$Y(\boldsymbol{\omega}) = \frac{1}{M} \sum_{\boldsymbol{m}_i \in \mathcal{N}(\boldsymbol{M}^T)} W(\boldsymbol{M}^{-T}(\boldsymbol{\omega} - 2\pi \boldsymbol{m}_i)), \tag{5}$$

where $M = \det |\boldsymbol{M}|$. This implies that $Y(\boldsymbol{\omega})$ is a sum of stretched and shifted versions of the original signal. Overlapping between these components result in aliasing error.

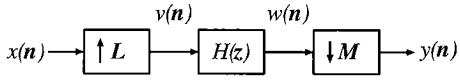

Fig. 1 Multidimensional sampling rate converter.

3. Checkerboard Distortion in Multidimensional Multirate Filters

3.1 Consideration in the Spatial Domain

Consider the polyphase decomposition of the impulse response $h(\boldsymbol{n})$ with respect to the sampling matrix $\boldsymbol{L}$;

$$r_{\boldsymbol{k}_i}(\boldsymbol{n}) = h(\boldsymbol{L}\boldsymbol{n} - \boldsymbol{k}_i) \tag{6}$$
$$(\boldsymbol{k}_i \in \mathcal{N}(\boldsymbol{L}),\ i = 1, \cdots L(= |\det \boldsymbol{L}|)).$$

By applying Eq. (6) to Fig. 1 and by using the *noble identity* [2], Fig. 1 is converted into Fig. 2, where $R_{\boldsymbol{k}_i}(\boldsymbol{z})$ is the z transform of the i-th polyphase component $r_{\boldsymbol{k}_i}$.

If the D-D step function

$$u(\boldsymbol{n}) = \begin{cases} 1 & (n_1, \cdots, n_D \geqq 0) \\ 0 & (\text{Otherwise}) \end{cases} \tag{7}$$

is fed as the input $x(\boldsymbol{n})$, the output of each path in Fig. 2 is given by

$$w_{\boldsymbol{k}_i}(\boldsymbol{n}) = \sum_{\boldsymbol{m} \in \mathcal{N}} r_{\boldsymbol{k}_i}(\boldsymbol{m}) \quad (\boldsymbol{k}_i \in \mathcal{N}(\boldsymbol{L})). \tag{8}$$

Note that the right hand side of Eq. (8) corresponds to the DC gain of the polyphase component $R_{\boldsymbol{k}_i}(\boldsymbol{z})$. Since these values are constants independently of $\boldsymbol{n}$, $w_{\boldsymbol{k}_i}(\boldsymbol{n})$ is written as $s_{\boldsymbol{k}_i}$ by dropping the spatial variable $\boldsymbol{n}$. If L values $s_{\boldsymbol{k}_1}, \cdots, s_{\boldsymbol{k}_L}$ are different one another, the output for such DC input involves spatially periodical distortion in relation to $\boldsymbol{L}$, which is known as *checkerboard distortion* because it can be seen like a checkerboard in the spatial domain.

On the contrary, it is easily confirmed that the downsampler $\boldsymbol{M}$ does not cause checkerboard distortion for the step input function. Therefore, it is concluded that checkerboard distortion for DC input can be avoided if the DC gain of each polyphase component $s_{\boldsymbol{k}_i}$ $(\boldsymbol{k}_i \in \mathcal{N}(\boldsymbol{L}))$ have the same value, from which we have

Theorem 1: The necessary and sufficient condition for the sampling rate converter shown in Fig. 1 to be checkerboard-distortion-free is that the DC gain of each polyphase component $s_{\boldsymbol{k}_i}$ $(\boldsymbol{k}_i \in \mathcal{N}(\boldsymbol{L}))$ has the same value.

Harada et al. have shown in Ref. [9] that a filter $H(\boldsymbol{z})$ can avoid checkerboard distortion if $H(\boldsymbol{z})$ is fac-

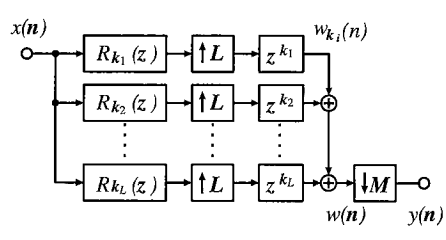

Fig. 2 Multidimensional sampling rate converter (polyphase decomposition).

torized as

$$H(\boldsymbol{z}) = P(\boldsymbol{z}) \sum_{\boldsymbol{k}_i \in \mathcal{N}(\boldsymbol{L})} \boldsymbol{z}^{-\boldsymbol{k}_i}, \tag{9}$$

where $P(\boldsymbol{z})$ is a linear time-invariant filter. The condition (9) is advantageous in the fact that it is structurally insensitive to coefficient quantization. This condition is, however, not a necessary and sufficient condition but only a sufficient condition. For example, in the case that $\boldsymbol{L} = \begin{bmatrix} 1 & 1 \\ 1 & -1 \end{bmatrix}$, the condition (9) implies that a checkerboard-distortion-free filter can be represented as

$$H(\boldsymbol{z}) = P(\boldsymbol{z})(1 + z_1^{-1}). \tag{10}$$

However, the filter

$$H(\boldsymbol{z}) = (z_2 + 2 + z_2^{-1})/4 \tag{11}$$

is not the case although it is checkerboard-distortion-free.

3.2 Consideration in the Frequency Domain

A necessary and sufficient condition for a 1-D multirate filter to be checkerboard-distortion-free has been derived in the frequency domain [6]–[8]. In this section, the similar condition is derived for the multidimensional case.

As discussed in Sect. 2, the upsampling process with $\boldsymbol{L}$ produces replica of the DC frequency at

$$\boldsymbol{\omega} = 2\pi \boldsymbol{L}^{-T} \boldsymbol{l}_j \quad (\boldsymbol{l}_j \in \mathcal{N}(\boldsymbol{L}^T),\ j \neq 1). \tag{12}$$

Due to such replica, checkerboard distortion is caused for DC input. Therefore, such distortion can be eliminated if the D-D multirate filter has zero on the frequency points given in Eq. (12). From this idea, we have the following theorem.

Theorem 2: The necessary and sufficient condition for the sampling rate converter shown in Fig. 1 to be checkerboard-distortion-free is that the frequency response $H(\boldsymbol{\omega})$ has zero at $\boldsymbol{\omega} = 2\pi \boldsymbol{L}^{-T} \boldsymbol{l}_j$ $(\boldsymbol{l}_j \in \mathcal{N}(\boldsymbol{L}^T),\ j \neq 1)$, i.e.,

$$H(\boldsymbol{\omega}) = 0 \quad (\boldsymbol{\omega} = 2\pi \boldsymbol{L}^{-T} \boldsymbol{l}_j,\ \boldsymbol{l}_j \in \mathcal{N}(\boldsymbol{L}^T),\ j \neq 1) \tag{13}$$

The proof for this theorem is given in Appendix A.

3.3 Error Analysis for Theorem 2

Even if a filter is designed so as to satisfy Theorem 2, coefficient quantization will violate the condition (13). This section gives an evaluation method for the effect of errors at the specified frequency points.

Here we assume that due to approximation error or coefficient quantization,

$$H(2\pi \boldsymbol{L}^{-T} \boldsymbol{l}_j) = \varepsilon_{\boldsymbol{l}_j} \quad (\boldsymbol{l}_j \in \mathcal{N}(\boldsymbol{L}^T),\ j \neq 1). \tag{14}$$

By replacing Eq. (A· 11) in the proof of Theorem 2 with

$$\boldsymbol{G} = [G,\ \varepsilon_{\boldsymbol{l}_2},\ \cdots,\ \varepsilon_{\boldsymbol{l}_L}], \tag{15}$$

we have

$$s_{\boldsymbol{k}_i} = \frac{1}{L}(G + \sum_{j=2}^{L} \varepsilon_{\boldsymbol{l}_j} e^{j2\pi \boldsymbol{l}_j^T \boldsymbol{L}^{-1} \boldsymbol{k}_i}). \tag{16}$$

Since

$$\left| \sum_{j=2}^{L} \varepsilon_{\boldsymbol{l}_j} e^{j2\pi \boldsymbol{l}_j^T \boldsymbol{L}^{-1} \boldsymbol{k}_i} \right| \leqq \sum_{j=2}^{L} \left| \varepsilon_{\boldsymbol{l}_j} \right|, \tag{17}$$

the following result can be obtained.

Theorem 3: In the case that Theorem 2 is not satisfied, the ratio of the maximum amplitude of checkerboard distortion and the DC gain of the frequency response $H(\boldsymbol{\omega})$ is bounded by $\left(\sum_{j=2}^{L} \left| \varepsilon_{\boldsymbol{l}_j} \right|\right)/G$.

3.4 Design of Multidimensional Multirate Filters without Causing Checkerboard Distortion

Since we have obtained Theorem 2, a checkerboard-distortion-free multirate filter can be basically designed simply by placing zero on suitable locations in the frequency domain.

Let $D(\boldsymbol{\omega})$ and $H_{\boldsymbol{c}}(\boldsymbol{\omega})$ be the frequency responses of the target and the filter to be designed, respectively, where $\boldsymbol{c}$ represents the coefficient vector to be determined. By taking Theorem 2 into account, the design problem can be formulated as

$$\min_{\boldsymbol{c}} \max_{\boldsymbol{\omega}} |D(\boldsymbol{\omega}) - H_{\boldsymbol{c}}(\boldsymbol{\omega})| \tag{18}$$

$$s.t.\ H_{\boldsymbol{c}}(2\pi \boldsymbol{L}^{-T} \boldsymbol{l}_j) = 0 \quad (\boldsymbol{l}_j \in \mathcal{N}(\boldsymbol{L}^T),\ j \neq 1). \tag{19}$$

Because Eqs. (18) and (19) can be converted into linear equations with respect to $\boldsymbol{c}$, they can be directly solved by using a linear programming package.

In the case that $SPD(\pi \boldsymbol{L}^{-T}) - 2\pi \boldsymbol{M}^{-T} \boldsymbol{m}_i$ $(\boldsymbol{m}_i \in \mathcal{N}(\boldsymbol{M}^T))$ does not overlap one another, Chen and Vaidyanathan's method [10] can be utilized. In their method, first 1-D prototype filter $P(\omega)$ with the passband in the section $-\pi/L \leqq \omega \leqq \pi/L$ is designed, and then the separable D-D filter $H'(\boldsymbol{\omega}) = \prod_{i=1}^{D} P(\omega_i)$ is calculated. Let $h'(\boldsymbol{n})$ be the impulse response of $H'(\boldsymbol{\omega})$. D-D filter with $SPD(\pi \boldsymbol{L}^{-T})$ being its passband can be obtained simply by downsampling the impulse response $h'(\boldsymbol{n})$ by $\hat{\boldsymbol{L}} = L\boldsymbol{L}^{-1}$. In this method, by designing $P(\omega)$ such that

$$P(\omega) = 0 \quad (\omega = 1\pi m/L,\ 1 \leqq m \leqq L), \tag{20}$$

the resulting filter satisfies Eq. (13), which guarantees the filter to be checkerboard-distortion-free. The proof of this sufficient condition is given in Appendix B.

4. Application to Scanning Line Conversion for TV Signals

As a practical example, the above results are applied to a scanning line converter for TV signals. An efficient implementation is also considered to reduce total amount of hardware.

4.1 Scanning Line Conversion by Multirate Filtering

In the current NTSC standard, the interlace scanning shown in Fig. 3 (a) has been adopted to reduce transmission bandwidth [4], which can be interpreted as a quincuncial sampling in the temporal–vertical 2-D plane. In order to accommodate to progressive-scanning displays, an interlace-to-progressive conversion is necessary, which corresponds to the sampling scheme conversion from quincuncial to orthogonal as shown in Fig. 3 (b) [4]. Another practical example for the sampling rate conversions in TV signal processing is to convert a 360-line signal in EDTV-II [11] into a conventional 480-line signal. This is nothing but a 1-D interpolating conversion in the vertical direction.

To realize the both conversions at a time, i.e. conversion from an interlaced 360-line (360i) signal to a progressive 480-line (480p) signal, $\boldsymbol{L}$ and $\boldsymbol{M}$ in Fig. 1 can be chosen such that

$$\boldsymbol{L} = \begin{bmatrix} 1 & 1 \\ 4 & -4 \end{bmatrix}, \quad \boldsymbol{M} = \begin{bmatrix} 1 & 0 \\ 0 & 3 \end{bmatrix} \tag{21}$$

as one of possible candidates. Figure 4 depicts the rearrangements of the sampling points in Fig. 1 in the temporal-vertical plane.

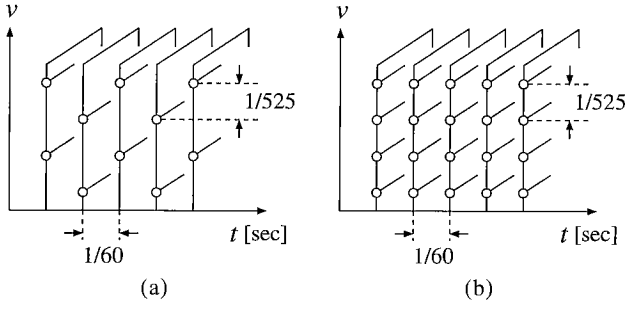

Fig. 3 Scanning in TV signal. (a) Interlace scanning. (b) Progressive scanning.

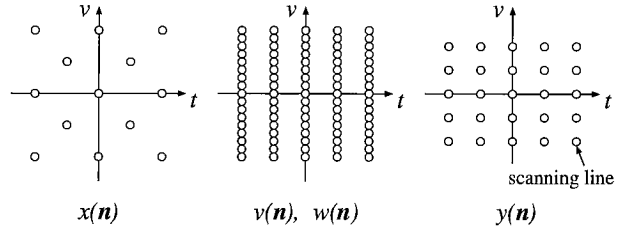

Fig. 4 Scanning line conversion from 360i to 480p in the temporal–vertical plane.

4.2 Reduction of the Number of Delay Elements in Polyphase-Decomposition-Based Implementation

By using multidimensional polyphase decomposition, the band-limiting filter $H(\boldsymbol{z})$ in Fig. 1 can be expressed as

$$\begin{aligned} H(\boldsymbol{z}) &= \sum_{\boldsymbol{n}\in\mathcal{N}} h(\boldsymbol{n})\boldsymbol{z}^{-\boldsymbol{n}} \\ &= \sum_{i=1}^{L}\left(\sum_{\boldsymbol{n}\in\mathcal{N}} h(\boldsymbol{Ln}-\boldsymbol{k}_i)\boldsymbol{z}^{-\boldsymbol{Ln}}\right)\boldsymbol{z}^{\boldsymbol{k}_i} \\ &= \sum_{i=1}^{L} R_{\boldsymbol{k}_i}(\boldsymbol{z}^{\boldsymbol{L}})\boldsymbol{z}^{\boldsymbol{k}_i} \quad (\boldsymbol{k}_i \in \mathcal{N}(\boldsymbol{L})), \end{aligned} \tag{22}$$

where $R_{\boldsymbol{k}_i}(\boldsymbol{z}^{\boldsymbol{L}})$ represents the polyphase component $\sum_{\boldsymbol{n}\in\mathcal{N}} h(\boldsymbol{Ln}-\boldsymbol{k}_i)\boldsymbol{z}^{-\boldsymbol{Ln}}$. With this decomposition, Fig. 1 can be converted into Fig. 2.

In designing the scanning line converter for TV signals, the axes n_1 and n_2 correspond to the temporal and vertical axes, respectively. The delay elements in these two directions are quite different from the viewpoint of hardware. Consider the case that NTSC signals are sampled with the sampling rate $4f_{sc}$, where f_{sc} is the color subcarrier frequency, i.e., 3.58 [MHz]. In this case, a single scanning line consists of 910 pixels and a single fields consists of 525/2 scanning lines [12], which implies that the unit delay in the temporal direction (field memory) is about 260 times more complex than that in the vertical direction (line memory). Therefore, from the viewpoint of hardware implementation, a reduction of the number of delays in the temporal direction, i.e, a reduction of field memories, is quite important. This section considers such a reducibility of the number of delay elements in 2-D sampling rate converters.

Assume, for example, that $\boldsymbol{L}$ and $\boldsymbol{M}$ are chosen as in Eq. (21) for Eq. (22) and that $\boldsymbol{k} = [k_{1i}, k_{2i}] \in \mathcal{N}(\boldsymbol{L})$. In this case, since $k_{1i} = -1$ $(i = 1, 2, \cdots, L)$, each $\boldsymbol{z}^{\boldsymbol{k}_i}$ $(i = 1, 2, \cdots, L)$ in Fig. 2 contains a single temporal delay. At the same time, each polyphase component $R_{\boldsymbol{k}_i}(\boldsymbol{z}^{\boldsymbol{L}}) = \sum h(\boldsymbol{Ln}-\boldsymbol{k}_i)\boldsymbol{z}^{-\boldsymbol{Ln}}$ requires a single additional temporal delay for implementation due to the shift by $\boldsymbol{k}_i$ in $h(\boldsymbol{Ln}-\boldsymbol{k}_i)$. As a result, this implementation totally requires $2L$ additional temporal delays. Although sharing the temporal delays is possible in $\boldsymbol{z}^{\boldsymbol{k}_i}$'s and $R_{\boldsymbol{k}_i}(\boldsymbol{z}^{\boldsymbol{L}})$'s, at least two additional temporal delays are inevitable. In what follows, a possibility of reducing the number of these additional delays is investigated.

Equation (22) can be further transformed into

$$\begin{aligned} &H(\boldsymbol{z}) \\ &= \sum_{i=1}^{L}\left(\sum_{\boldsymbol{n}\in\mathcal{N}} h(\boldsymbol{L}(\boldsymbol{n}+\boldsymbol{n}_i')-(\boldsymbol{k}_i+\boldsymbol{Ln}_i'))\right. \end{aligned}$$

$$\cdot z^{-\boldsymbol{L}(\boldsymbol{n}+\boldsymbol{n}_i')}\Big)z^{\boldsymbol{k}_i+\boldsymbol{L}\boldsymbol{n}_i'} \quad (\boldsymbol{n}_i' \in \mathcal{N}). \tag{23}$$

A replacement of

$$\boldsymbol{k}_i' = \boldsymbol{k}_i + \boldsymbol{L}\boldsymbol{n}_i' \quad \boldsymbol{n}'' = \boldsymbol{n} + \boldsymbol{n}_i' \tag{24}$$

in Eq. (23) leads to

$$\begin{aligned} H(z) &= \sum_{i=1}^{L}\left(\sum_{\boldsymbol{n}''\in\mathcal{N}} h(\boldsymbol{L}\boldsymbol{n}''-\boldsymbol{k}_i')z^{-\boldsymbol{L}\boldsymbol{n}''}\right)z^{\boldsymbol{k}_i'} \\ &= \sum_{i=1}^{L} R_{\boldsymbol{k}_i'}(z^{\boldsymbol{L}})z^{\boldsymbol{k}_i'} \\ &= \sum_{i=1}^{L} R_{\boldsymbol{k}_i'}(z^{\boldsymbol{L}})z_1^{k_{1i}'}z_2^{k_{2i}'}, \end{aligned} \tag{25}$$

where $\boldsymbol{k}_i' = [k_{1i}', k_{2i}']^T$. From Eq. (25), we have the following result.

Theorem 4: Let $\boldsymbol{L} = \begin{bmatrix} l_{11} & l_{12} \\ l_{21} & l_{22} \end{bmatrix}$ in Eqs. (24) and (25). By suitably selecting $\boldsymbol{n}_i'$ $(i = 1, \cdots, L)$ in Eq. (24), we can make the vector $\boldsymbol{k}_i'$ such that

$$|k_{1i}'| < GCM(l_{11}, l_{12}) \tag{26}$$

or

$$|k_{2i}'| < GCM(l_{21}, l_{22}), \tag{27}$$

where $GCM(x, y)$ represents the greatest common measure of x and y.

The proof of this theorem will be given in Appendix C.

Theorem 4 implies that, if l_{11} and l_{12} are mutually prime or $l_{11} = l_{12} = 1$, the filter can be implemented without using the delay element for n_1. Because Eq. (21) corresponds to the latter case, by selecting $\boldsymbol{n}_i' = [-1, -4]^T$, the band-limiting filter $H(\boldsymbol{z})$ can be written as

$$H(\boldsymbol{z}) = \sum_{k_2'=0}^{L-1} R_{[0\ -k_2']^T}(z^{\boldsymbol{L}})z_2^{-k_2'}. \tag{28}$$

This transformation saves $2L$ additional temporal delays (field memories) in Fig. 2, compared with the implementation with $\boldsymbol{n}_i = [0, 0]$. Figure 5 (a) shows the implementation based on Eq. (28). In Fig. 5 (a), the right part consisting of the upsamplers, the delay chain, and the downsampler works as a selector for the polyphase components on a vertical line, which puts the output of each polyphase component on the suitable place. By taking such an operation into account, Fig. 5 (a) can be rewritten as in Fig. 5 (b). This shows that the essential part of the proposed implementation is in the selection of the polyphase components satisfying Eq. (26).

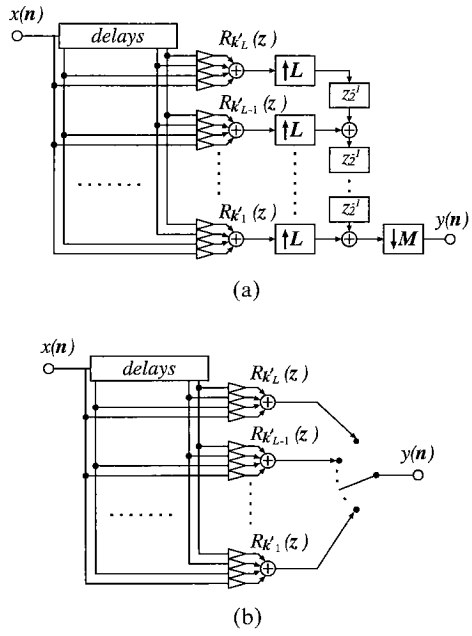

Fig. 5 Implementation of the scanning line converter with considering Theorem 4. (a) Circuit derived from Fig. 2. (b) Equivalent circuit.

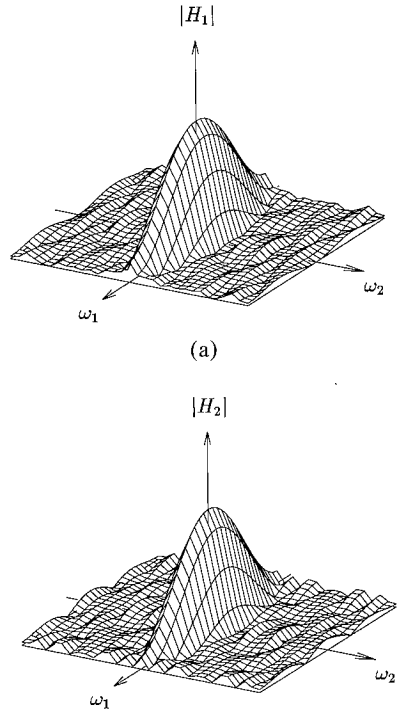

Fig. 6 Designed band-limiting filter for the 360i-to-480p conversion. (a) and (b) have been designed with and without the condition (20), respectively.

(a)

(b)

Fig. 7 Results of the 360i-to-480p conversion. (a) and (b) are the results by the filters H_1 and H_2, respectively.

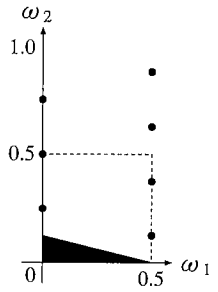

Fig. 8 Specifications for the band-limiting filter. Only the first quadrant is shown here.

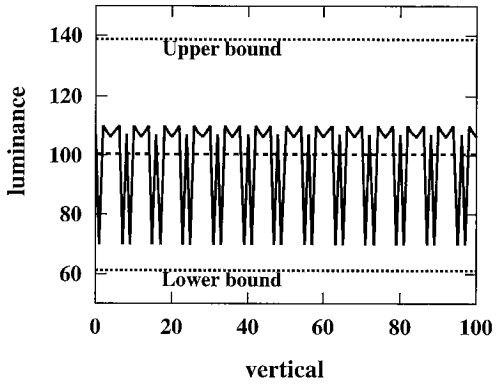

Fig. 9 Luminance variation by checkerboard distortion.

4.3 Experiment

This section gives experimental results of the scanning line conversion for Eq. (21). Since Eq. (21) causes no overlapping between the spectrum $SPD(\pi \boldsymbol{L}^{-T}) - 2\pi \boldsymbol{M}^{-T}\boldsymbol{m}_i$ $(\boldsymbol{m}_i \in \mathcal{N}(\boldsymbol{M}^T))$, the band-limiting filter $H(\boldsymbol{z})$ can be designed by Chen and Vaidyanathan's method. The 1-D prototype FIR filter having its passband in the section $-\pi/8 \leqq \omega \leqq \pi/8$ is first designed with the length 23. Then, the production filter is downsampled by $\boldsymbol{L}$ in Eq. (21), which produces a 5×23-tap 2-D filter. As discussed in Sect. 3.4, by taking the condition (20) into account, a checkerboard-distortion-free filter can be designed, which is referred to as $H_1(\boldsymbol{z})$ later on. Figure 6 (a) shows the frequency response of the designed band-limiting filter $H_1(\boldsymbol{z})$. Figure 6 (b) also shows the same filter designed without considering the condition (2), which is referred to as $H_2(\boldsymbol{\omega})$.

Figure 7 shows the results of 360i to 480p conversion by the both filters. There is no checkerboard distortion in the result by H_1 while heavy checkerboard distortion can be seen in that by H_2. Although the zeros required by Theorem 2 are all located in the stopband as shown in Fig. 8, small approximation error remains on each point without the condition (20). From Eq. (17), these small errors pile up to cause heavy distortion. To evaluate the validity of Eq. (17), an image with constant luminance 100 is fed to the converter with H_2. Figure 9 shows the luminance variation along with a vertical line at the output. The upper and lower bounds are calculated from Eq. (17). We can confirm that Eq. (17) gives a relatively good bound for the amplitude of checkerboard distortion. These result show the importance of zeros that Theorem 2 requires for the band-limiting filters in multirate systems.

5. Conclusion

In this paper, checkerboard distortion in multidimensional multirate filters has been considered. By investigating checkerboard distortion in the both spatial and frequency domains, the necessary and sufficient conditions which avoid checkerboard distortion were derived. Since the condition in the frequency domain is related to the location of zeros of the band-limiting filter, the effect of the error at the required zeros was investigated to obtain a bound for the amplitude of checkerboard distortion.

Then, the derived conditions were applied to a scanning line converter for television signals. Because, in this case, a reduction of the number of delay elements with respect to one of the axes is quite important, the reducibility was also discussed from the implementation viewpoint. Finally, in order to confirm the obtained re-

sults, a scanning line conversion was performed by using the band-limiting filters with and without considering the derived condition. The results clearly illustrate the importance of zeros required in certain points in the frequency domain. By incorporating the motion adaptation technique proposed by the authors [13], practical scanning line converters can be designed.

References

[1] R.E. Crochiere and L.R. Rabiner, "Multirate Digital Signal Processing," Englewood Cliffs, Prentice-Hall, 1983.
[2] P.P. Vaidyanathan, "Multirate Systems and Filter Banks," Englewood Cliffs, Prentice-Hall, 1993.
[3] H. Kiya, "Adaptive signal processing using filter banks: Subband adaptive filters," The Journal of IEICE, vol.79, no.2, pp.169–172, 1996.
[4] T. Fukinuki, "Multi-dimensional TV signal processing," Nikkan–Kogyo–shimbunsha, Nov. 1989.
[5] M. Kato, T. Yoshida, and A. Nishihara, "Design of multirate filters with time-domain constraints," IEICE Technical Report, CAS96-4, June 1996.
[6] M. Kato, T. Yoshida, and A. Nishihara, "Necessary and sufficient condition for M-channel perfect reconstruction filter banks to avoid checkerboard effects," IEICE Technical Report, CAS96-79, Jan. 1997.
[7] M. Kato, "Study on the design of multirate systems without causing checkerboard effects," Master Thesis in Tokyo Inst. of Tech., Feb. 1997.
[8] Y. Harada and H. Kiya, "Multirate filter without checkerboard effect and its zero point location," IEICE Technical Report, CAS96-78, Jan. 1997.
[9] Y. Harada, S. Muramatsu, and H. Kiya, "Checkerboard effects in multidimensional multirate systems," IEICE Technical Report, CAS97-26, June 1997.
[10] T. Chen and P.P. Vaidyanathan, "Multidimensional multirate filters and filter banks derived from one-dimensional filters," IEEE Trans. Signal Processing, vol.41, no.5, pp.1749–1765, May 1993.
[11] S. Kikuchi and M. Hatori, "Making process of EDTV-II technical standard," The Journal of ITE, vol.49, no.9, pp.1117–1120, Sept. 1995.
[12] T. Yoshida, K. Ashizawa, and A. Nishihara, "Design of YC separation filters," IEEE Trans. Circuits & Systs for Video Tech., vol.2. no.4, pp.373–380, Dec. 1992.
[13] T. Tamura, T. Yoshida, A. Nishihara, and Y. Sakai, "Scanning line conversion of moving images using 2-D multirate filters," Proc. of 12th DSP Symposium, pp.549–554, Nov. 1997.

Appendix A: Proof of Theorem 2

Since the frequency response of $H(\boldsymbol{z})$ can be written as

$$H(\boldsymbol{\omega}) = \sum_{\boldsymbol{n}\in\mathcal{N}} h(\boldsymbol{n}) e^{-\jmath\boldsymbol{\omega}^T\boldsymbol{n}}, \tag{A·1}$$

a substitution of $\boldsymbol{\omega} = 2\pi\boldsymbol{L}^{-T}\boldsymbol{l}_j$ $(\boldsymbol{l}_j \in \mathcal{N}(\boldsymbol{L}^T), j = 2, \cdots, L)$ leads to

$$H(2\pi\boldsymbol{L}^{-T}\boldsymbol{l}_j) = \sum_{\boldsymbol{n}\in\mathcal{N}} h(\boldsymbol{n}) e^{-\jmath 2\pi\boldsymbol{l}_j^T\boldsymbol{L}^{-1}\boldsymbol{n}} \quad (\boldsymbol{l}_j \in \mathcal{N}(\boldsymbol{L}^T), j \neq 1). \tag{A·2}$$

By converting Eq. (A·2) into the polyphase representation,

$$H(2\pi\boldsymbol{L}^{-T}\boldsymbol{l}_j) = \sum_{i=1}^{L}\Big(\sum_{\boldsymbol{n}\in\mathcal{N}} h(\boldsymbol{L}\boldsymbol{n}+\boldsymbol{k}_i) \cdot e^{-\jmath 2\pi\boldsymbol{l}_j^T\boldsymbol{L}^{-1}(\boldsymbol{L}\boldsymbol{n}+\boldsymbol{k}_i)}\Big). \tag{A·3}$$

Since $e^{-\jmath 2\pi\boldsymbol{l}_j^T\boldsymbol{n}} = 1$ for integer vectors $\boldsymbol{l}_j$ and $\boldsymbol{n}$, Eq. (A·3) is simplified into

$$H(2\pi\boldsymbol{L}^{-T}\boldsymbol{l}_j) = \sum_{i=1}^{L}\Big(\sum_{\boldsymbol{n}\in\mathcal{N}} h(\boldsymbol{L}\boldsymbol{n}+\boldsymbol{k}_i) \cdot e^{-\jmath 2\pi\boldsymbol{l}_j^T\boldsymbol{L}^{-1}\boldsymbol{k}_i}\Big). \tag{A·4}$$

By the definition of $s_{\boldsymbol{k}_i}$, Eq. (A·4) can be transformed into

$$H(2\pi\boldsymbol{L}^{-T}\boldsymbol{l}_j) = \sum_{i=1}^{L} s_{\boldsymbol{k}_i} e^{-\jmath 2\pi\boldsymbol{l}_j^T\boldsymbol{L}^{-1}\boldsymbol{k}_i}. \tag{A·5}$$

Consider the case

$$s_{\boldsymbol{k}_1} = s_{\boldsymbol{k}_2} = \cdots = s_{\boldsymbol{k}_L}. \tag{A·6}$$

In this case, Eq. (A·5) can be written as

$$H(2\pi\boldsymbol{L}^{-T}\boldsymbol{l}_j) = s_{\boldsymbol{k}_1}\sum_{i=1}^{L} e^{-\jmath 2\pi\boldsymbol{l}_j^T\boldsymbol{L}^{-1}\boldsymbol{k}_i}. \tag{A·7}$$

Since

$$\sum_{i=1}^{L} e^{-\jmath 2\pi\boldsymbol{l}_j^T\boldsymbol{L}^{-1}\boldsymbol{k}_i} = \begin{cases} L & (j=1) \\ 0 & (j\neq 1) \end{cases} \tag{A·8}$$

holds [2], Eq. (A·7) leads to

$$H(2\pi\boldsymbol{L}^{-T}\boldsymbol{l}_j) = 0 \tag{A·9}$$

for $\boldsymbol{l}_j \in \mathcal{N}(\boldsymbol{L}^T)$, $(j \neq 1)$.

Conversely, consider the case that $H(\boldsymbol{\omega})$ has zero on $\boldsymbol{\omega} = 2\pi\boldsymbol{L}^{-T}\boldsymbol{l}_j$ $(\boldsymbol{l}_j \in \mathcal{N}(\boldsymbol{L}^T), j \neq 1)$. Equation (A·5) can be represented in the matrix form as

$$\boldsymbol{W}\boldsymbol{s} = \boldsymbol{G}, \tag{A·10}$$

where

$$\boldsymbol{s} = [s_{\boldsymbol{k}_1}, \cdots, s_{\boldsymbol{k}_L}]^T, \quad \boldsymbol{G} = [G, 0, \cdots, 0]^T \tag{A·11}$$

and G is the DC gain of $H(\boldsymbol{\omega})$. $\boldsymbol{W}$ in Eq. (A·10) is the $L \times L$ generalized DFT matrix [2] whose element is given by

$$[\boldsymbol{W}]_{ij} = e^{-\jmath 2\pi\boldsymbol{l}_j^T\boldsymbol{L}^{-1}\boldsymbol{k}_i} \quad (\boldsymbol{k} \in \mathcal{N}(\boldsymbol{L})). \tag{A·12}$$

From Eq. (A·8), $\boldsymbol{W}$ is an unitary matrix satisfying

$$\boldsymbol{W}^\dagger\boldsymbol{W} = L\boldsymbol{I}, \tag{A·13}$$

where $\boldsymbol{W}^{\dagger}$ represents the conjugate transpose of $\boldsymbol{W}$. From Eq. (A· 13), we have

$$\boldsymbol{W}^{-1} = L^{-1}\boldsymbol{W}^{\dagger}. \tag{A· 14}$$

By using this relation,

$$\boldsymbol{s} = \boldsymbol{W}^{-1}\boldsymbol{G} = L^{-1}\boldsymbol{W}^{\dagger}\boldsymbol{G} \tag{A· 15}$$

is obtained from Eq. (A· 10). Since the first row of $\boldsymbol{W}^{\dagger}$ is $[1, 1, \cdots, 1]$.

$$s_{\boldsymbol{k}_i} = L^{-1}G \quad (1 \leqq i \leqq L) \tag{A· 16}$$

can be shown.

Appendix B: Proof of the Sufficient Condition (20)

Let $H'(\boldsymbol{\omega}) = \prod_{i=1}^{D} P(\omega_i)$ be the separable D-D filter obtained from the 1-D prototype $P(\omega)$ which has its passband in the section $-\pi/L \leqq \omega \leqq \pi/L$ and satisfies Eq. (20). According to the Chen and Vaidyanathan's method, the desired multirate filter $H(\boldsymbol{\omega})$ can be obtained simply by downsampling the impulse response of $H'(\boldsymbol{\omega})$ by $\hat{\boldsymbol{L}} = L\boldsymbol{L}^{-1}$. We have to show here is that the resulting filter $H(\boldsymbol{\omega})$ has zeros at $\boldsymbol{\omega}$'s given in Eq. (12).

From Eq. (5),

$$H(\boldsymbol{\omega}) = \frac{1}{\hat{L}} \sum_{\hat{\boldsymbol{l}}_i \in \mathcal{N}(\hat{\boldsymbol{L}}^T)} P(\hat{\boldsymbol{L}}^{-T}(\boldsymbol{\omega} - 2\pi\hat{\boldsymbol{l}}_i)), \tag{A· 17}$$

where $\hat{L} = |\det \hat{L}|$. A substitution of Eq. (12) leads to

$$H(2\pi\boldsymbol{L}^{-T}\boldsymbol{l}_j) = \frac{1}{\hat{L}} \sum_{\hat{\boldsymbol{l}}_i \in \mathcal{N}(\hat{\boldsymbol{L}}^T)} P\left(\frac{2\pi}{L}(\boldsymbol{l}_j - \boldsymbol{L}^T\hat{\boldsymbol{l}}_i)\right) \quad (j = 2, \cdots L). \tag{A· 18}$$

Since the elements of $\boldsymbol{l}_j$, $\boldsymbol{L}^T$ and $\hat{\boldsymbol{l}}_i$ are all integers, each element of the vector $\boldsymbol{l}_j - \boldsymbol{L}^T\hat{\boldsymbol{l}}_i$ is also an integer, which guarantees that each element of $\frac{2\pi}{L}(\boldsymbol{l}_j - \boldsymbol{L}^T\hat{\boldsymbol{l}}_i)$ is a multiple of $\frac{2\pi}{L}$.

This proof completes if it is shown that all the elements of the vector $\frac{2\pi}{L}(\boldsymbol{l}_j - \boldsymbol{L}^T\hat{\boldsymbol{l}}_i)$ never become an integer multiple of 2π at the same time. This can be shown easily. Since $\hat{\boldsymbol{l}}_i$ is an integer vector, $\boldsymbol{L}^T\hat{\boldsymbol{l}}_i \in LAT(\boldsymbol{L}^T)$. Now consider the lattice $LAT(L\boldsymbol{I})$ where $\boldsymbol{I}$ is the identity matrix. Since a lattice point in $LAT(L\boldsymbol{I})$, i.e. $L\boldsymbol{I}\boldsymbol{n}$ $(\boldsymbol{n} \in \mathcal{N})$ can be written as

$$\begin{aligned} L\boldsymbol{I}\boldsymbol{n} &= L(\boldsymbol{L}^T\boldsymbol{L}^{-T})\boldsymbol{n} = \hat{\boldsymbol{L}}^T(L\boldsymbol{L}^{-T})\boldsymbol{n} \\ &= \boldsymbol{L}^T(\hat{\boldsymbol{L}}\boldsymbol{n}), \end{aligned} \tag{A· 19}$$

$LAT(L\boldsymbol{I}) \subset LAT(\hat{\boldsymbol{L}}^T)$. $\boldsymbol{L}^T\hat{\boldsymbol{l}}_i \in LAT(L\boldsymbol{I})$ is also obtained because $\boldsymbol{L}^T\hat{\boldsymbol{L}}^T = L\boldsymbol{I}$. But since $\boldsymbol{l}_j$ is an integer vector in $FPD(\boldsymbol{L}^T)$ and $\boldsymbol{l}_j \neq \boldsymbol{0}$ for $j = 2, \cdots L$, $\boldsymbol{l}_j \notin LAT(\boldsymbol{L}^T)$. By combining these,

$$\boldsymbol{l}_j - \boldsymbol{L}^T\hat{\boldsymbol{l}}_i \notin LAT(L\boldsymbol{I}) \tag{A· 20}$$

holds for $j = 2, \cdots, L$ and $i = 1, 2, \cdots L$, which guarantees that all the elements of $\frac{2\pi}{L}(\boldsymbol{l}_j - \boldsymbol{L}^T\hat{\boldsymbol{l}}_i)$ never become an integer multiple of 2π at the same time.

From the above results and from Eq. (20), we can prove that the resulting filter $H(\boldsymbol{\omega})$ has zero at $\boldsymbol{\omega}$'s given in Eq. (12).

Appendix C: Proof of Theorem 4

Here we prove Eq. (26). Equation (27) can be proven in the same way. Let $\boldsymbol{L}$ be the integer matrix

$$\boldsymbol{L} = \begin{bmatrix} l_{11} & l_{12} \\ l_{21} & l_{22} \end{bmatrix}, \tag{A· 21}$$

and let

$$\boldsymbol{n}' = \begin{bmatrix} n_1' \\ n_2' \end{bmatrix} \quad (\boldsymbol{n}' \in \mathcal{N}) \tag{A· 22}$$

$$\boldsymbol{k}_i = \begin{bmatrix} k_{i1} \\ k_{i2} \end{bmatrix} \quad (\boldsymbol{k}_i \in \mathcal{N}(\boldsymbol{L}), 1 \leqq i \leqq L). \tag{A· 23}$$

By selecting

$$\boldsymbol{k}_i' = \begin{bmatrix} k_{i1}' \\ k_{i2}' \end{bmatrix} = \boldsymbol{k}_i + \boldsymbol{L}\boldsymbol{n}', \tag{A· 24}$$

we have

$$k_{i1}' = k_{i1} + n_1'l_{11} + n_2'l_{12}. \tag{A· 25}$$

[I] In the case that l_{11} and l_{12} are mutually prime.

From the Euclidean algorithm, we can find the integer p and q which satisfy

$$pl_{11} + ql_{12} = 1. \tag{A· 26}$$

By setting

$$n_1' = -k_{i1}p, \quad n_2' = -k_{i1}q \tag{A· 27}$$

for the obtained p and q, $k_{i1}' = 0$ holds because of Eqs. (A· 25) and (A· 26).

[II] In the case that l_{11} and l_{12} are not mutually prime.

Let $g(> 0)$ be the greatest common measure of l_{11} and l_{12}. Then, by using mutually prime integers l_{11}' and l_{12}',

$$l_{11} = gl_{11}', \quad l_{12} = gl_{12}'. \tag{A· 28}$$

Again from Euclidean algorithm, we can find the integer p and q which satisfy

$$pl_{11}' + ql_{12}' = 1 \tag{A· 29}$$

$$pl_{11} + ql_{12} = g. \tag{A· 30}$$

By setting

$$n_1' = mp, \; n_2' = mq \tag{A· 31}$$

with an integer m, we have

$$k_{i1}' = k_{i1} + mg \tag{A· 32}$$

from Eqs. (A· 25), (A· 30), and (A· 31). By suitably selecting m,

$$|k'_{i1}| < g \qquad \text{(A· 33)}$$

is obtained.

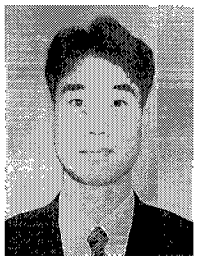

Tomohiro Tamura received B.E. and M.E. in electronics from Tokyo Inst. of Tech. in 1996 and 1998, respectively. He is now with Sony Corporation and is engaged in designing broadcasting monitors. During his student days in Tokyo Inst. of Tech., he was engaged in the research of digital signal processing.

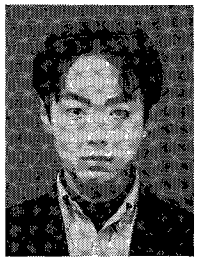

Masaki Kato received B.E. and M.E. in electronics from Tokyo Inst. of Tech. in 1995 and 1997, respectively. During his student days in Tokyo Inst. of Tech., he was engaged in the research of multirate signal processing. He is currently employed by Texas Instruments Japan Limited, where he has been working on DVD LSI development at DVD Prodcuts Division.

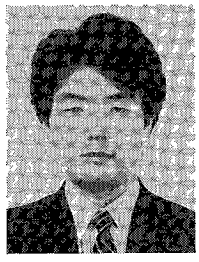

Toshiyuki Yoshida received B.E., M.E, and D.E. all from Tokyo Inst. of Tech. in 1986, 1988, and 1991, respectively. Since then he has been with Tokyo Inst. of Tech., where he is now an associate professor of Dept. of Physical Electronics. His research interests are in the area of image processing and multidimensional signal processing.

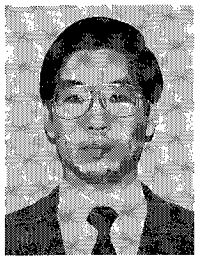

Akinori Nishihara received the B.E., M.E. and Dr. Eng. degrees in electronics from Tokyo Inst. of Tech. in 1973, 1975 and 1978, respectively. Since 1978 he has been with Tokyo Inst. of Tech., where he is now Professor of the Center for Research and Development of Educational Technology (CRADLE). His main research interests are in filter design, 1-D and multi-D signal processing, and educational technology. He is now serving as Editor-in-Chief of the Trans. IEICE A (in Japanese). Dr. Nishihara is a member of IEEE, EURASIP, ECS and JET.